Journal of Materials Chemistry B

Computational Design to Experimental Validation: Molecular Dynamics-assisted Development of Polycaprolactone Micelles for Drug Delivery†

Journal:	*Journal of Materials Chemistry B*
Manuscript ID	TB-ART-12-2024-002789.R1
Article Type:	Paper
Date Submitted by the Author:	10-Feb-2025
Complete List of Authors:	Stefan, Mihaela; The University of Texas at Dallas, Chemistry and Biochemistry Grabowski, Gerik; The University of Texas at Dallas, Chemistry and Biochemistry Shah, Tejas; The University of Texas at Dallas, Chemistry and Biochemistry Polara, Himanshu; The University of Texas at Dallas, Chemistry and Biochemistry Babanyinah, Godwin; The University of Texas at Dallas, Chemistry and Biochemistry Bhadran, Abhi; The University of Texas at Dallas, Chemistry and Biochemistry Wang, Hanghang; University of Texas at Dallas, Chemistry Cu Castillo, Cristina; University of Texas at Dallas, Department of Chemistry Biewer, Michael; University of Texas at Dallas, Department of Chemistry Torabifard, Hedieh; The University of Texas at Dallas, Chemistry and Biochemistry

ARTICLE

Received 00th January 20xx,
Accepted 00th January 20xx

DOI: 10.1039/x0xx00000x

Computational Design to Experimental Validation: Molecular Dynamics-assisted Development of Polycaprolactone Micelles for Drug Delivery†

Tejas Shah,‡[a] Himanshu Polara,‡[a] Godwin Babanyinah,[a] Abhi Bhadran,[a] Hanghang Wang,[a] Cristina Cu Castillo,[a] Gerik Grabowski,[a] Michael C. Biewer,[a] Hedieh Torabifard,*[a] and Mihaela C. Stefan*[a]

Amphiphilic diblock copolymers are used in drug delivery systems for cancer treatments. However, these carriers suffer from lower drug loading capacity, poor water solubility, and non-targeted drug release. Here, we utilized a computational approach to analyze the effect of the functional group of the hydrophobic block on the drug-polymer interactions. To design effective drug carriers, four different amphiphilic block copolymer micelles with aromatic and heteroaromatic groups at the hydrophobic core were subjected to molecular dynamics simulations. The solvent-accessible surface area, water shell, hydrogen bonding, and radius of gyration of the simulated micelles were determined. Further, we assessed the interactions between the hydrophobic block and drug molecules using linear interaction energy and non-covalent interactions. The computational studies revealed that the micelles containing a novel γ-2-methoxyfuran-ε-caprolactone (FuCL) hydrophobic have the highest polymer-drug interactions. From these findings, we synthesized a novel amphiphilic Poly(ethylene glycol)-*b*-poly(γ-2-methoxyfuran(ε-caprolactone) (PEG-*b*-PFuCL) using ring-opening polymerization of FuCL monomer. The polymer was self-assembled in aqueous media to form micelles. The aromatic segment of PEG-*b*-PFuCL micelles enhanced the doxorubicin (DOX) loading through non-covalent interactions, resulting in a 4.25 wt% drug-loading capacity. We also showed that the hydrolysis of the ester bond allowed a faster in vitro drug release at pH 5.0 compared to pH 7.4. Cell viability experiments revealed that DOX-loaded PEG-*b*-PFuCL micelles show that micelles are cytotoxic and readily uptaken into MDA-MB-231 cells. Therefore, furan-substituted micelles will be an ideal drug carrier with higher polymer-to-drug interactions, enhanced drug loading, and lower premature leakage.

Introduction

Despite the extensive research on novel cancer drugs and treatments, finding an efficient cure for cancer remains one of the major challenges in medicinal chemistry. This is partly due to issues such as low water-solubility, poor biodistribution, pharmacokinetics, and bioavailability of anticancer drugs in vivo, as well as the lack of specificity and limited understanding of tumor physiology. As a result, significant efforts have been made to develop improved drug delivery systems using nanotechnology to improve the overall therapeutic efficiency of anticancer drugs.[1-3] Therefore, materials that are biocompatible, biodegradable, and nontoxic are desired for drug delivery applications.[4-7]

Aliphatic polyesters are among the extensively studied polymers for drug delivery applications due to their biodegradability, biocompatibility, and good mechanical

[a] Department of Chemistry and Biochemistry, University of Texas at Dallas, Richardson, TX, USA. E-mail: Hedieh.Torabifard@UTDallas.edu, Mihaela@UTDallas.edu.
‡ These authors contributed equally to this work
* Corresponding authors
† Supplementary Information available: Snapshots of the simulation progress of micelles with different functional groups, synthesis process, NMR of monomers and polymers, and SEC of homopolymer and copolymer. See DOI: 10.1039/x0xx00000x

properties.[4-6] Among these, poly(ε-caprolactone) (PCL) offers several advantages, including tailorable degradation kinetics, processability, and ease of functionalization, which makes it an ideal candidate for drug delivery applications.[8-10] Specifically, the micellar drug delivery carriers obtained from the amphiphilic diblock copolymers of PCL are currently under intense investigation.[8-10] The unique core-shell structure of the micelles protects the hydrophobic drug from aqueous media, thereby enhancing the circulation of the drug in the bloodstream. The specificity of these formulations is enhanced by exploiting the enhanced permeability and retention (EPR) effect by restricting the micellar diameter to less than 200 nm.[11-13] Moreover, the γ-position of ε-caprolactone (CL) monomer can be easily modified, which also provides an opportunity to tailor the properties of diblock copolymers. This functionalization changes the polymerization kinetics and physicochemical properties of the polymer, and in the context of drug delivery, is also amenable to incorporating drugs, bioactive moieties, and reactive components.[14,15] Our group has capitalized on this approach to tailor the properties of resultant micelles for drug delivery applications for cancer treatment.[4,16-22]

Despite the advantages mentioned above, micellar drug delivery systems still face significant challenges. This includes poor in vivo stability, premature drug release, and inadequate drug loading to achieve sufficient therapeutic efficacy. Extensive efforts and strategies have been employed to enhance the micelle stability and drug loading capacity. Most of these issues can be addressed by judicious design of the hydrophobic block, controlling the molecular weight, and optimizing the hydrophilic to hydrophobic block ratio. Since the drug is encapsulated in the core, engineering the hydrophobic core of the micelle plays an essential role in the performance of the micellar drug delivery system.[23-28] The hydrophobic functional groups that participate in non-covalent interactions with the drug molecules promote the drug loading capacity (DLC) of the micelles.[13] This strategy is much more feasible and avoids concerns of additional toxicities and the pharmaceutical performance of the drugs since drug molecules are chemically unaltered. The classic approach for higher drug-polymer interaction is to incorporate aromatic groups into the polymeric backbone. These aromatic functional groups at the micellar core can orient themselves to enhance π–π stacking with aromatic drug molecules, such as doxorubicin (DOX). The loading capacity is further augmented since other forces can coexist with π–π interactions.[29-31] We have demonstrated four to five-fold higher DLC by co-loading polyphenol (quercetin and resveratrol, respectively) and doxorubicin (DOX) anticancer drug, which exploits the hydrogen-bonding and π–π interactions between the polyphenols and DOX.[16,20] The number of aromatic pendant group can be increased by preparing star-like topology of polymers.[32] For example, Buwalda *et al*[33] reported a 8-arm PEG-*b*-PCL star polymer with benzylthiother functionality to achieve 9.7% loading of curcumin. However, the performance of these flower-like micelles was hampered by low critical aggregation concentration, size distribution and slow drug release.

The ever-increasing chemical diversity with sophisticated nanotechnology available for drug formulation should provide researchers with a suitable arsenal to develop a myriad of novel drug delivery systems. However, the absence of mechanistic insights into the driving forces within micellar drug delivery systems results in heavy reliance on experimental screenings. While valuable, these screenings are time- and resource-intensive, leading to limited cases of alternative delivery systems used in commercially available therapeutics.[34-36] It is, therefore, essential to optimize the development of the screening process, which integrates the complementary in silico methods such as molecular dynamics (MD) simulations. However, studying micellar systems using full atomistic simulations is challenging due to its sheer computational costs. To circumvent this problem, coarse-grained and dissipative particle dynamics models have been reported.[34,37-40] Although these models provide valuable insights, they lack detailed information such as interatomic interactions.[34,37-40] These interatomic interactions are necessary for the micelles functioning as a drug delivery carriers, and therefore, full atomistic MD simulations are necessary.[41,42] The all-atom MD simulations have been employed to study micelles composed of amphiphilic poly(N-isopropyl acrylamide)-*b*-poly(ethylene glycol) copolymer for the curcumin delivery.[43] The study, however, lacked a thorough investigation of drug-polymer interaction. We have previously reported a protocol to simulate full-atomistic models of γ-functionalized CL-based amphiphilic polymeric micelles. In our approach, we scaled the charges of the hydrophilic block of the polymer and simulated truncated polymer chains to show that the model can capture the aggregation behavior and polymer-drug interactions throughout the simulations by utilizing the power of Graphics processing unit (GPU) processors.[44]

Herein, we report a computational approach for the rational design of micellar drug delivery systems. We modeled four micelles containing distinct functional groups, namely-cyclopentane (CP), cyclopentadiene (CPD), furan (Fu), and thiophene (Th) linked through ether functional group on PCL backbone of the hydrophobic block and poly(ethylene glycol) (PEG) was used as a hydrophilic block (**Figure 1A**). These functional groups are chosen to capture the impact of aromaticity and heteroatom of the aromatic ring on the drug-polymer interactions and ease of synthesis. The heterocyclic compounds represent a significant class of organic compounds with considerable biological and industrial applications. Due to their unique properties, they are fundamental blocks of natural products such as nucleic acids, amino acids, carbohydrates, vitamins, and alkaloids.[45-49] We simulated all the micelles for 100 ns and determined the aggregation behavior, solvent-polymer interaction, and, more importantly, drug-polymer interactions. From the data obtained from the simulation, we selected the best-performing polymer, synthesized and characterized it experimentally. The micelles from the synthesized diblock amphiphilic polymer were prepared, and DOX was encapsulated to determine the drug-loading capacity of the micelles. Further, in vitro drug release and cytotoxicity on MDA-MB-231 breast cancer cells were also determined. The

principal idea of this work is to design an amphiphilic block copolymeric micellar carrier that has straightforward synthesis, has a good drug loading capacity and are capable of accumulating inside the cancer cells *via* EPR effect.

Experimental

Materials and Characterization

All the chemicals were purchased from Fisher Scientific or Sigma-Aldrich and used without purification except tin(II) 2-ethylhexanoate ($Sn(Oct)_2$) that was purified through vacuum distillation. The ring-opening polymerization was carried out under a nitrogen atmosphere in toluene obtained from the Inert MD5 solvent purification system. Schlenk flask and syringes used were left overnight at 120 °C and cooled in a desiccator before use for polymerization. Synthesis of the monomer and the polymerization were carried out by slightly modifying our previously published procedures,[4,16-18,20,30,50,51] a detailed procedure of monomer synthesis is available in SI†.

The ^{1}H and ^{13}C NMR spectroscopy for all the monomers, precursors, and the resulting polymers were carried out using Bruker AVANCE III^{TM}(500 MHz) nuclear magnetic resonance (NMR) instrument in deuterated chloroform (CDCl3) at 25 °C. Viscotek VE 3580 size exclusion chromatography (SEC) with Viscotek columns (T6000M) and a refractive index (RI) detector was used to determine the polydispersity index (Đ) and the number average molecular weights of the polymers. HPLC grade THF was used as the eluent at a flow rate of 1 mL min^{-1} at 30 °C with GPC max as the sample module with polystyrene standards. The dynamic light scattering (DLS) measurements were carried out using a Malvern Zetasizer instrument with a 4 mW He–Ne laser (633 nm) and an avalanche photodiode (APD) detector. Measurements were obtained with a detector angle of 173° at 25 °C. A JEM-1400+ TEM (JEOL USA Inc., MA) microscope was employed to record TEM images. TEM samples were prepared by treating the copper mesh grid with 1 mg mL^{-1} micelle solution for 2 min, then stained with 2 wt% Phosphotungstic acid for 1 min. Cytotoxicity measurements were obtained with a BioTek Cytation 3 multi-mode reader, and cellular uptake images were obtained from EVOS FL digital inverted fluorescence microscope.

Molecular Dynamics Simulation

Force Field Development

The force field parameters were obtained by dividing each polymer into four fragments (**Figure 1**). These fragments were prepared in Gaussview06[52] and individually optimized using HF/6-31G(d) method in Gaussian16[53] to be compatible with version 2 of General Amber Force Fields (GAFF2).[54] The Antechamber[55]-derived fragmental charges with AM1-BCC[56,57] method for the hydrophilic block, were inadequate to impart water-solubility, as reported in our previous work.[44] Hence, the hydrophilicity of the polymer block was adjusted by scaling the charges of the hydrophilic fragments. Finally, the amphiphilic polymer chain having 14 units of PEG and 9 units of the hydrophobic block was obtained by uniting the fragments without the capping groups in the Leap utility with the GAFF2 force field. The parameters of the DOX molecule were obtained from our previously reported work.[44]

Modeling DOX-loaded micelles

The diblock copolymer obtained by joining the fragments was non-linear. An optimized linear polymer chain was obtained by performing a short vacuum simulation, and the coordinates of the straight polymer were obtained. The Polymer-DOX systems were prepared in packmol[58] functionality with 25 optimized chains with hydrophobic blocks facing towards the center of the sphere. The final system had ~10 wt% (12) DOX molecules with a distance of at least 5 Å from the polymeric chains in a 50 Å radius sphere. This configuration was selected to promote the micellization and DOX-polymer interaction. The final polymer-drug system was solvated with 10 Å buffer in TIP3P[59] water with periodic boundary conditions.

Simulation Details

For all the simulations, GPU-supported AMBER20[60] package with GAFF2[54] parameters was employed. The simulations were caried out using the protocol reported by our group previously.[44] Briefly, the systems were 1) energy minimized twice with a restraint of 40 kcal/mol/$Å^2$ on the polymer backbone and the PEG-block, respectively, followed by 2) NVT equilibration, 3) NPT equilibration, and 4) NPT production. After the minimization system was gradually heated in NVT ensemble using Langevin dynamics[61] and equilibrated in NPT ensemble with a restraint (40 kcal/mol/$Å^2$) on PEG-block. Finally, unrestrained systems were simulated for 105 ns using Langevin dynamics[61] and a collision frequency of 1.0 ps^{-1} in NPT conditions with Langevin thermostat[61] and Berendsen barostat.[62] The information about all the systems with simulation times are outlined in **Table 1**. The simulations were run with the SHAKE algorithm[63] at a timestep of 2 fs with a distance cutoff of 12 Å, with trajectories saved every 20 ps. The long-range Coulomb interactions were treated using the particle mesh Ewald (PME) method.[64] All the simulations were performed at the atmospheric pressure and at 300 K. All the simulations were triplicated for sampling and statistical analysis.

The visualization of the simulation trajectories was performed with the VMD program.[65] The CPPTRAJ program was utilized to carry out all the analyses[66], except drug-polymer intermolecular hydrogen bonds, which were determined from the VMD.[65] The results do not include the first 5 ns of the production time to achieve equilibration of the simulated polymer-drug system.

The percent dehydration of the micelles was calculated by computing the ratio of the polymer-polymer hydrogen bond (n_{pp}) to polymer-polymer hydrogen bond and water-polymer hydrogen bond (n_{pw}).[67]

$$\%\text{Dehydration} = \frac{n_{pp}}{n_{pp} + n_{pw}} \times 100$$

The non-covalent interaction (NCI) plots were obtained by choosing two regions of the polymer fragments within 5 Å of encapsulated DOX molecules from the final frame. The images were generated from the Multiwfn code developed by Lu and Chen.[68]

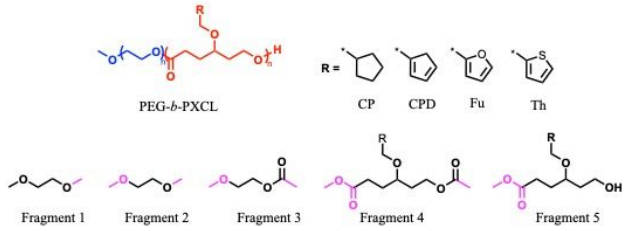

Figure 1. Structures of (A) simulated amphiphilic block copolymers and (B) the structural representation of the fragments for force field parametrization. These fragments were then joined to prepare PEG-b-PXCL polymers for MD simulation. The atoms colored magenta in the fragments were removed to make a copolymer. Abbreviations used: cyclopentane (CP), cyclopentadiene (CPD), furan (Fu), and thiophene (Th).

Polymerization

Synthesis of homopolymer

To an oven-dried 10 mL Schlenk flask, dried monomer (0.1 g, 0.477 mmol), benzyl alcohol (0.052 g, 0.005 mmol) and $Sn(Oct)_2$ (0.00193 g, 0.005 mmol) in dry toluene (0.2 mL) were added inside a nitrogen-filled glove box. The flask was sealed and placed in a preheated oil bath at 110 °C. The ^{1}H NMR spectroscopy was utilized to monitor monomer consumption, which was fully consumed after 16 h of reaction. The mixture was cooled to room temperature and dissolved by adding a few drops of THF. The polymer was reprecipitated in cold methanol. The process was repeated thrice, and the vacuum-dried homopolymer was obtained as a yellow viscous liquid (yield= 68%). ^{1}H NMR (500 MHz, $CDCl_3$) δ 1.75-1.9 (m, 4H), 2.3-2.35 (m, 2H), 3.5-3.6 (m, 1H), 4.1-4.15 (m, 2H), 4.45 (s, 2H), 5.1 (s, 2H), 6.35-6.40 (dd, 1H), 6.45 (dd, 1H), 7.4 (dd, 1H). ^{13}C NMR δ 28.02, 29.35, 34.19, 61.43, 64.97, 74.86, 109.35, 110.52, 143.02, 151.81, 176.09, 183.17.

Synthesis of block copolymer

To an oven-dried 10 mL Schlenk flask, dried monomer (0.5 g, 2.38 mmol), PEG2000 (0.095 g, 0.048 mmol), and $Sn(Oct)_2$ (0.0193 g, 0.048 mmol) in dry toluene (0.5 mL) were added inside a nitrogen-filled glove box. The sealed flask was placed in a preheated thermostat-controlled oil bath at 110 °C. The monomer consumption was monitored using ^{1}H NMR spectroscopy, and the monomer was consumed fully after 16 h of reaction. The mixture was then cooled to room temperature and dissolved by adding a few drops of THF, and the polymer was reprecipitated in cold methanol. The process was repeated thrice, and the obtained polymer was dried under vacuum to yield PEG-*b*-PFuCL as a viscous liquid (yield= 71%). $CDCl_3$) δ ^{1}H NMR 1.75-1.89 (m, 4H), 2.3-2.35 (m, 2H), 3.38 (m, 3H), 3.5-3.65 (m, 1H), 3.65 (s, 4H), 4.1-4.15 (m, 2H), 4.45 (s, 2H), 6.35-6.40 (dd, 1H), 6.45 (dd, 1H), 7.4 (dd,1H). ^{13}C NMR δ 28.99, 29.63, 33.03, 50.99, 61.17, 63.19, 70.53, 74.49, 109.19, 110.28, 142.79, 151.87, 173.38.

Preparation of empty and loaded micelles

The detailed procedure for preparing DOX-loaded micelles is previously reported.[17,18,30] Briefly, DOX solution was prepared by neutralizing 1 mg mL^{-1} DOX · HCl solution in THF with 3 eq. of triethylamine. DOX-loaded micelles with a polymer-to-DOX weight ratio of 10:1 were prepared by mixing 0.5 mL of DOX solution and 5 mg PEG-*b*-PFuCL dissolved in THF. This mixture was dropwise added to 5 mL DI water and homogenized for 30 min, and the traces of THF gradually evaporated using a vortex mixer. The micelle solution was dialyzed using a dialysis bag (SnakeSkin®, cutoff size 3500 Da) with 500 mL DI water. for 24 hours. The dialysis media was replenished every 8 hours to withdraw unencapsulated DOX and fractions of THF. The obtained DOX-loaded micelles solution was filtered through a Nylon syringe filter (size 0.22 µm), and the drug loading capacity (DLC) and efficiency (DLE) of the micelles were determined using the following equation.

$$\text{DLC} = \frac{\text{Weight of DOX loaded}}{\text{weight of total polymer}} \times 100$$

$$\text{DLE} = \frac{\text{Weight of DOX loaded}}{\text{weight of total DOX}} \times 100$$

The empty micelles were obtained using a similar approach without adding DOX. The size and morphology of both empty and DOX-loaded micelles were determined.

Critical micelle concentration

The critical micelle concentration (CMC) of the amphiphilic diblock copolymer was determined through fluorescence microscopy using pyrene as the hydrophobic probe.[17,69,70] For this study, serial concentrations (1×10^{-7} mg mL^{-1} to 1×10^{-1} mg mL^{-1}) of the polymer were prepared in 10 mL water and 25 µL of pyrene solution with constant concentration was added to each solution. The solution obtained was vortexed to remove any residual THF. The excitation spectra of the pyrene were taken at an emission of 390 nm for each solution using a fluorescence spectrometer. The CMC was determined by plotting the ratio of the intensity at 338 nm to 334 nm (I_{338}/I_{334}) against the log of the polymer concentration.

Size and morphology of the micelles

The micelle size was determined using a DLS instrument. Before analysis, the micelles were prepared in DI water at 1.0 mg mL^{-1} concentration. The prepared samples were equilibrated at 25 °C using a Malvern Zetasizer Nano ZS instrument to measure the hydrodynamic diameters (Dh) of the micelles. Morphological investigations of the micelle solution were conducted using TEM. A 2wt% phosphotungstic acid (PTA) solution was used to stain the micelles for morphology analysis. For this, 10 µL sample and 10 µL of PTA were placed individually on a parafilm. The sample was covered by laying a dark side of the glow-discharged copper mesh for 2 minutes, followed by stain exposure for 1 minute. The excess solution from the grid was removed by gently dabbing the edge with filter paper. The

Table 1. Outline of the simulations and analysis conducted.

Functional Group	Box Size (Å³)	Total Atoms	Total Simulation Time (ns)	Analysis
Cyclopentane (CP)	181 × 168 × 195	524, 719	300	SASA, water contact, H-bond, R_g, lie, NCI
Cyclopentadiene (CPD)	164 × 180 × 165	426, 961	300	SASA, water contact, H-bond, R_g, lie, NCI
Furan (Fu)	186 × 152 × 182	446, 134	300	SASA, water contact, H-bond, R_g, lie, NCI
Thiophene (Th)	137 × 155 × 141	256, 162	300	SASA, water contact, H-bond, R_g, lie, NCI

Drug release study

The *in vitro* pH-dependent DOX release from the polymeric micelles was determined at physiological conditions (pH of 7.4, 37 °C) and tumor-mimicking environment (pH 5.0, 37 °C) in phosphate buffer solution (PBS). A dialysis bag (cutoff 3500 Da) containing 4 mL DOX-loaded micelles solution was incubated in 10 mL PBS for both pH conditions, and the amount of the released DOX was calculated with UV-vis analysis. The withdrawn media was replaced with 0.3 mL fresh media. Each sample was diluted with DMSO and was subjected to UV–vis spectroscopy to quantify the amount of DOX released based on the pre-established calibration curve. The cumulative release of DOX was calculated using the equation below, where m_0 is the amount of DOX released into the media, V_0 and V_e are the volumes of the release media (10.0 mL) replaced media (0.3 mL), respectively. C_i is the DOX concentration in the release media, C_n is the concentration of DOX in the sample.

$$\text{Cumulative release of DOX (\%)} = \frac{V_e \sum_1^{n-1} C_i + V_0 C_n}{m_0} \times 100\%$$

Cell culture

MDA-MB-231 cells (ATCC® HTB-26TM) were cultured (37 °C in 5% CO_2 conditions) in Dulbecco's Modified Eagle Medium (DMEM, Sigma-Aldrich), 10% fetal bovine serum (FBS, GibcoTM, Fisher Scientific) and 1.0% penicillin/streptomycin (GibcoTM, 10,000 U mL–1, Sigma-Aldrich) and routinely sub-cultured at ca. 80% confluency. 4',6-diamidino-2-phenylindole (DAPI), and 3-(4,5-dimethylthiazol-2-yl)-2,5-diphenyltetrazolium bromide (MTT) were purchased from Fisher Scientific or Sigma-Aldrich.

Cytotoxicity assay

MDA-MB-231 Breast cancer cells were supplemented with DMEM, 10% FBS, and 1.0% penicillin/streptomycin. The cells were seeded in a 96-well plate, each with 1×10^4 cells. The cells were allowed to attach to the wells by incubating at 37 °C, 5% CO_2 for 24 h. The culture media was substituted with fresh media and then treated with 50 µL solution of empty and DOX-loaded micelles at distinct concentrations (0.03 to 0.50 mg mL^{-1} in PBS). 50 µL PBS was added to the control cells, and cells were incubated in the same conditions for another 24 h. After rinsing the cells with 100 µL PBS, 30 µL of 12mM MTT solution was added, and the formation of formazan crystals was allowed by incubating cells for 4 h. The formazan crystals were dissolved in 170 µL DMSO. The absorption was recorded at 570 nm and normalized to the intensity of the control cells (N = 3, standard deviation). The statistical analysis was performed in Excel using one-way ANOVA. The *p*-values of ≤ 0.05 were statistically significant.

Cellular uptake

In a 35 mm 24-well plate, cells were grown at a cell density of 1×10^5 cells per well and incubated for 24 h. The culture media was replaced, and 100 µL DOX-loaded micelles (0.50 mg mL^{-1}) with fresh media were added to the cells. After 4 h of further incubation, the media was emptied, cells were washed thrice with PBS and fixed with 100 µL 4.0% paraformaldehyde. After 10 minutes of incubation, the cells were washed again with PBS three times before staining the nucleus with DAPI according to the protocol recommended by the manufacturer. The images of the cellular uptake of the micelles were taken using EVOS FL digital inverted fluorescence microscope.

Results and discussion

Molecular Dynamics Simulation of DOX-loaded Micelles

Amphiphilic diblock copolymer PEG-*b*-poly(ε-caprolactone) with four different functional groups (**Figure 1A**) at the γ-position of the CL monomer were simulated to design the efficient micellar drug delivery carrier. The structure of all the polymer chains, regardless of the functional group, was optimized by simulating them in the vacuum for a very short (0.5 ns) time. The coordinates of the structure when the block copolymer begins to straighten up were saved and used to make initial structures. Given the coiling tendency of the polymer chain, the length of the polymer chains differed by a small amount. However, the block copolymer containing the Th functional group started coiling during the structure optimization. Hence, the starting structure of the block polymeric chains with Th functional chain has a smaller simulation box and, ultimately, fewer atoms (due to fewer water molecules required for solvation) (**Table 1**). Although full-atomistic simulations provide a clearer picture of the atomistic models, they are computationally expensive. Hence, we conducted our simulations with truncated chain polymeric chains to reduce the computational cost without losing information on atomistic interactions. For this study, block polymers with a 14-unit long PEG block and a 9-unit long hydrophobic block were prepared. The length of PEG was intentionally kept longer than the hydrophobic block to provide enough hydrophilicity and colloidal stability to the micelles. The initial simulations with AM1-BCC charge methods did not give the expected aggregation behavior. Therefore, the charges of the hydrophilic fragment were increased by 10%. Our previous report thoroughly discusses the optimization of block length, the number of polymeric chains, and the charge scaling of hydrophilic blocks.[44] Briefly, we simulated polymer fragments and water interface, and if the fragments didn't mix with water,

we gradually increased the charges (to increase the hydrophilicity of the fragment). This process was repeated until the hydrophilic fragments were mixed with water, and it was determined that charge increment by 10% provides hydrophilicity to the PEG block. The amended charges provided spherical micelles with all four functional groups (**Figure S1-S4**†). The polymer chains began coiling in the NPT equilibration step with micellization around 15 ns of production simulation time. The encapsulation of DOX molecules in the micelles was observed within the first 20 ns of the production, showing the proclivity of drug molecules to interact with the hydrophobic block. However, the coiling of the polymer chains was faster than the drug encapsulation; hence, some drug molecules were found to be at the surface of the micelle. The shape of the micelles and drug encapsulation is qualitatively consistent with previously reported studies for PEG-containing micelles and our previous studies.[43,44,71-73]

SASA, watershell and R_g of drug-loaded micelles

To determine how the aggregation of the chain impacts the exposure of polymeric chains to the solvent media, we determined the SASA of the micelles (**Figure S5-S6**†). The Fu group containing micelles showed the lowest SASA values (average SASA= 261.67 ± 25.26 nm^2) followed by the Th group containing micelles (average SASA= 286.87 ± 20.27 nm^2). The CP group containing micelles, which is non-aromatic, has the highest SASA values, suggesting that the micelles containing aromatic-functional groups (Fu, Th, CPD) are compact and have the least exposure to solvent media. Micellar carriers act as a solubility medium for a hydrophobic drug; hence, exposure of the drug to the water media is an essential parameter for a drug delivery carrier. We calculated the solvent-accessible surface area (SASA) of the encapsulated DOX molecules in all simulated polymers (**Figure 2**). As expected, the SASA values of the drug molecules were 10 times lower than that of SASA values for the micelles. The DOX encapsulated in micelles with Fu functional group had the lowest SASA values (average SASA 23.41 ± 4.97 nm^2). The SASA values of DOX molecules encapsulated in CP and CPD groups containing micelles were nearly similar (average

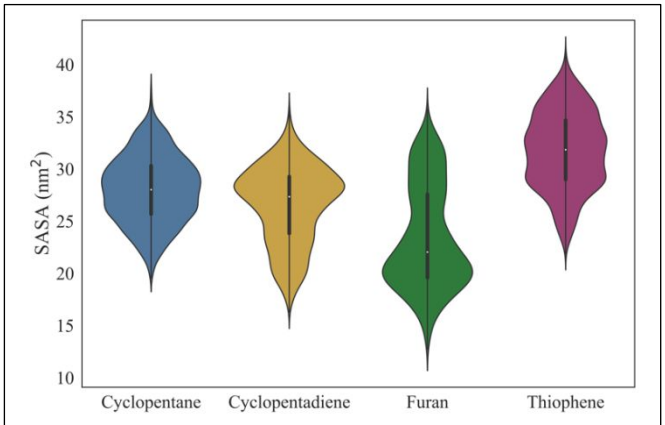

Figure 2. Violin plots of solvent accessible surface area (SASA) of the DOX molecules in the simulated polymers. The median of all three trials is represented by the white dot. All groups are statistically significant (p <0.001).

SASA values 28.01 ± 3.20 nm^2 and 26.54 ± 3.74 nm^2, respectively). Interestingly, the Th group containing micelles provided the highest SASA values for encapsulated DOX (31.84 ± 3.72 nm^2). This might be due to the considerable difference in size between the heteroatom in the aromatic ring and carbon, oxygen, and nitrogen atoms in DOX molecules. The oxygen atom in Fu, on the other hand, is shown to favor interaction by electrostatics and dipole moment.[74] This has been further observed in linear interaction energy (lie) analysis, which will be discussed later. We also determined the number of water molecules $N_{(H2O)}$ within the 3.5 Å of the individual blocks of the micelles as the simulation progressed (**Figure 3**). As expected, the number of water molecules around the hydrophilic block was more than twice that of the hydrophobic block, suggesting that the hydrophobic block aggregated tightly, forming the core of micelles. The $N_{(H2O)}$ of a hydrophobic block in all the micelles is similar, with micelles containing the Th group being slightly lower than other functional groups (**Figure 3A**). This could be because the Th-containing polymer chain started coiling during optimization, resulting in fewer water molecules in the

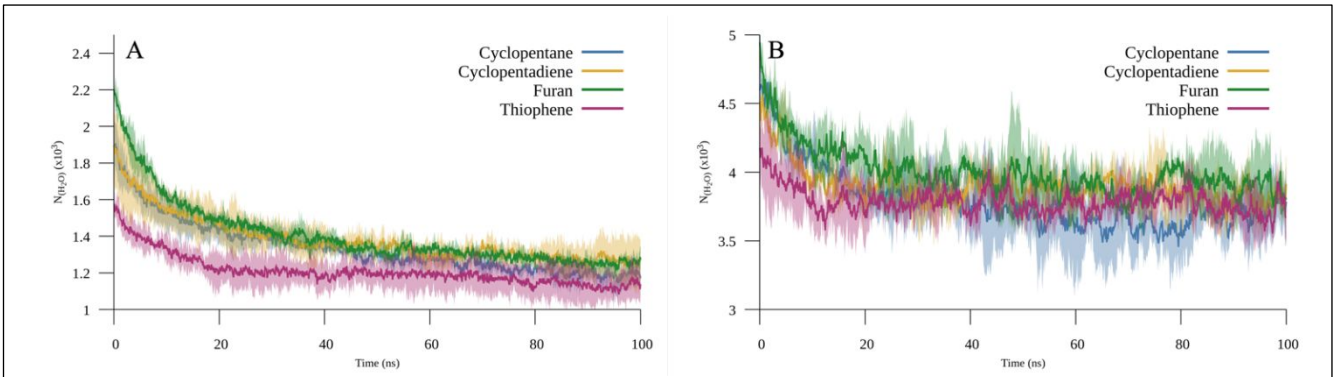

Figure 3. Comparison of the total number of water molecules within 3.5 Å of the (A) hydrophobic block and (B) hydrophilic block of simulated micelles. The standard deviation of all the trials is represented by a shaded region, and the solid line shows the average number of water molecules over three trials.

simulation box (**Table 1**). Further, the micelles started aggregating during the equilibration stage, which further lessened the surrounding N. This could be clearly seen in (**Figure 3**) where a $N_{(H2O)}$ around Th-group containing micelles were smaller from the beginning compared to micelles with other functional groups. A close examination of the trend of the hydrophilic block shows that the $N_{(H2O)}$ remained nearly the same after an initial drop, suggesting the tendency of the hydrophilic block to interact with surrounding water molecules. This indicates that the modified parameters for hydrophilic fragments provide the necessary hydrophilicity to the block. The $N_{(H2O)}$ for hydrophilic blocks for all the micelles has a similar behavior with slight deviation throughout the simulation. This is because although the micelles differ in their hydrophobic functional group, they possess the same hydrophilic block in all the micelles. The number of water molecules around the micelles at a longer distance (5 Å) was also determined (**Figure S7**†), and it showed a similar trend.

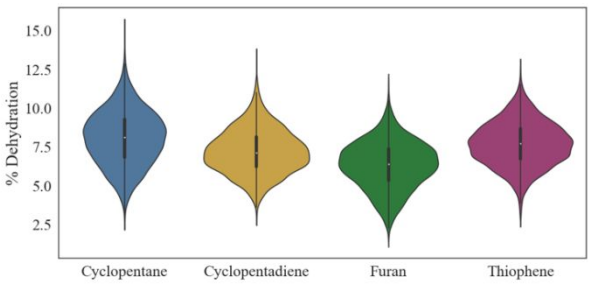

Figure 4. Violin plots of the dehydration percentage of the hydrophobic core of the simulated micelles. The median of all three trials is represented by the white dot.

The dehydration percentage of the micelles was also determined (**Figure 4**), which shows that all the micelles dehydrated nearly similarly. The micelles bearing Fu functional group had slightly less dehydration number. This may be due to the hetero oxygen atom in the ring being capable of interacting with hydrogen atoms of the water molecules.

To determine the compactness of the formed micelles, we calculated the radius of gyration (R_g) of the micelles for the last 60 ns of production. Regardless of the functional group, all the micelles showed bimodal or trimodal distribution of R_g with nearly similar average R_g values, ranging from 24.61 to 27.05 Å (**Figure S8**†), except the micelles containing the CP functional group. which showed a wide distribution of R_g values consistent with SASA analysis. The bimodal distribution is also observed for micelles containing Fu and Th functional groups, albeit with the lower R_g values, i.e., compact micelles.

Interaction of functional groups with drug molecules

The interaction between drugs and polymers is a critical factor in determining the properties of micellar drug carriers. To determine which functional group will be better suited for the drug delivery application, we characterized the drug-polymer interaction of all the simulated micelles using linear interaction energy (lie) analysis, which calculates the non-bonded (vdw and coulomb) interaction energies over the simulation trajectory. First, we determined the total interaction between the hydrophobic block of the polymer chains and DOX molecules (**Figure S9**†). The micelles bearing Fu functional groups show the highest interaction with the DOX molecules, followed by the micelles containing CPD functional group. Interestingly, the micelles containing Th functional group showed the least total interaction with the DOX molecules. To obtain further insights into non-bonded interactions, we plotted van der Waals (vdW) and electrostatic (Coulomb) interactions against simulation time (**Figure 5**). The plots suggest that vdW interactions significantly contribute to drug encapsulation in all polymers. The micelles containing Th and CP functional groups had the least vdW and electrostatic interaction. The CP functional group is not aromatic and is, therefore, unable to induce π–π interaction with DOX molecules. On the other hand, in the aromatic Th group, the interaction is hampered by faster chain aggregation compared to the other micelles and poor overlapping of sulfur heteroatom with DOX molecules. This was further confirmed in watershell analysis, where the Th group containing micelles had the highest SASA and least water molecules. Surprisingly, the values of vdW interactions of micelles containing CPD and Fu group were similar. This is because although Fu group is aromatic, it has more resemblance to diene, and CPD group allows better overlap with DOX due to the absence of heteroatom. However, the electrostatic interactions of micelles containing the Fu group

were higher than those of the CPD functional group (**Figure 5B**), making its interaction with DOX more favorable.

We further analyzed the nature of non-bonded interactions using non-covalent interactions (NCI) analysis using Multiwfn code, using reduced density gradient method. NCI analysis is a qualitative method to identify non-covalent interactions between interacting molecules. The output file contains colored surfaces between molecules, and the color codes represent the strength of interaction (**Figure 6)**.[68,75] The NCI analyses are shown in **Figure 6, Figures S10-S13**†. The CP functional groups show a little overlapping with DOX molecules (**Figure S10**†), and only London forces seem to play a role in the drug encapsulation. Other groups show better overlapping and have weak interactions with DOX molecules (**Figure 6, Figures S9-S12**†). The CPD and Th groups were found to have T-shaped stacking (right column **Figure 6A and C**), though there were fewer Th groups around the DOX molecules than the CPD groups. This could be due to the faster coiling of polymer chains containing Th functional group. The Fu functional groups were found to form $\pi-\pi$ interactions with DOX by face-to-face stacking (showed in circle in **Figure 6**), off-centered stacking (circled in **Figures S12**†) and T-shaped stacking (right column **Figure 6B**). It has been suggested that the T-shaped and off-centered stacking is favored mode of interaction compared to face-to-face interaction.[76] This explains the formation of compact micelles with stronger drug-polymer interactions in the micelles containing Fu pendant group throughout our MD simulations.

To assess the electrostatic interactions, we calculated the number of hydrogen bonds ($N_{(H\text{-}bonds)}$) formed between the hydrophobic block of the micelles and drug molecules (**Figure 7**). The H-bonds are expected to be responsible for the majority of electrostatic interaction observed in lie analysis (**Figure 5B**), and indeed, the H-bond analysis follows a similar order as observed in the lie analysis. The hydrophobic block with Fu functional groups forms the highest number of the H-bonds with the DOX molecules.

ARTICLE

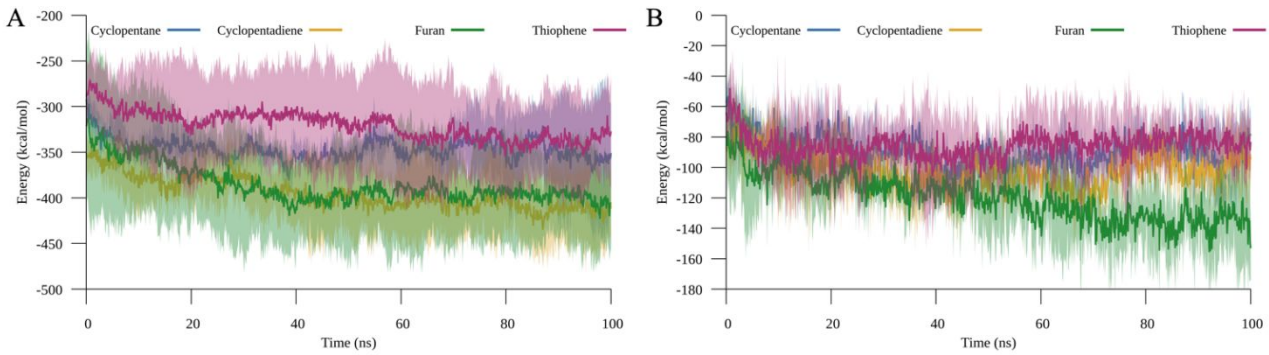

Figure 5. The time evolution of DOX-polymer (A) vdW and (B) Coloumb interaction. The average of three trials is represented by a solid line, while the standard deviations are represented by a shaded region.

Overall, the results of SASA, watershell, R_g, and interaction analysis of the micelles containing Fu functional group showed highest interaction with DOX molecules, lesser SASA values of DOX molecules, and were more compact than other functional groups. This augmented interaction via both π-π interactions and hydrogen bonding, is expected to encapsulate more DOX with smaller micellar size. Therefore, we opted to synthesize PEG-*b*-PFuCL micelles and characterize them to assess their potential for drug delivery applications.

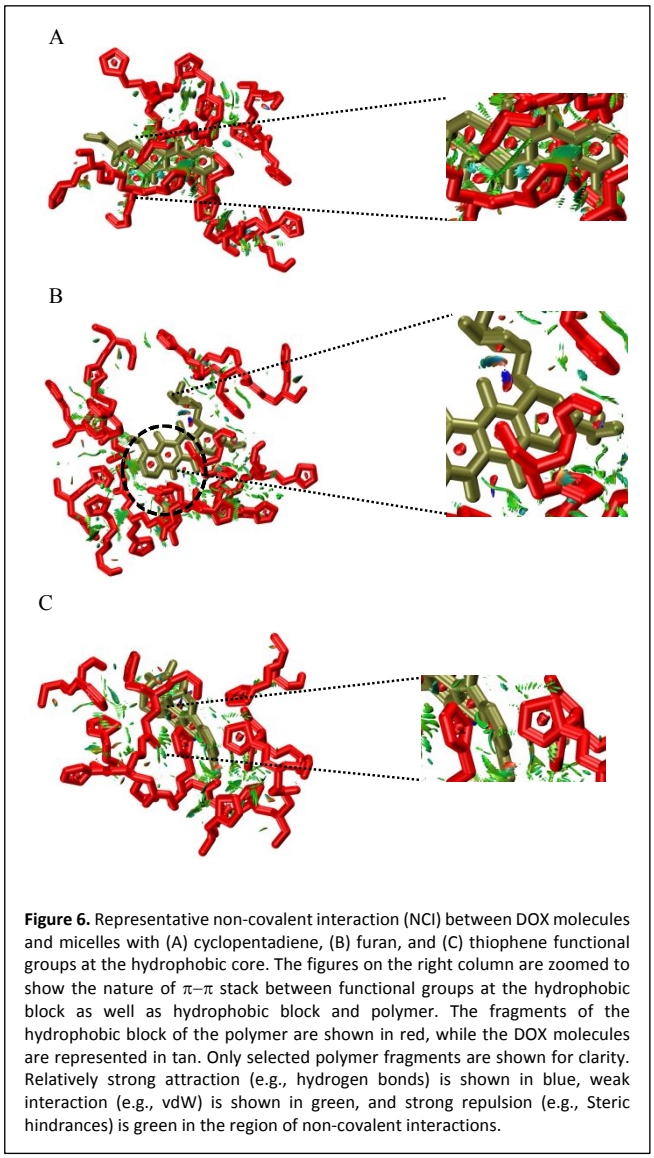

Figure 6. Representative non-covalent interaction (NCI) between DOX molecules and micelles with (A) cyclopentadiene, (B) furan, and (C) thiophene functional groups at the hydrophobic core. The figures on the right column are zoomed to show the nature of π–π stack between functional groups at the hydrophobic block as well as hydrophobic block and polymer. The fragments of the hydrophobic block of the polymer are shown in red, while the DOX molecules are represented in tan. Only selected polymer fragments are shown for clarity. Relatively strong attraction (e.g., hydrogen bonds) is shown in blue, weak interaction (e.g., vdW) is shown in green, and strong repulsion (e.g., Steric hindrances) is green in the region of non-covalent interactions.

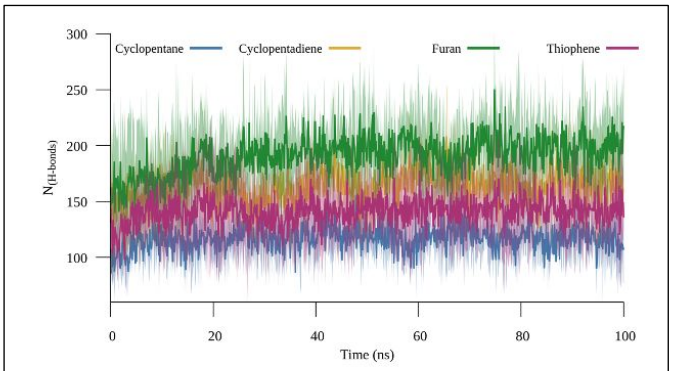

Figure 7. The time plot of number of H-bonds between encapsulated DOX in the simulated micelles. The average of three trials is shown by solid line and standard deviation is shown by shaded region.

Synthesis of FuCL

Synthesis of monomer

The FuCL monomer was synthesized by modifying the method reported by our group (**Scheme S1**†).[4] Initial efforts were made to obtain bromo- and tosylate-derivative of 2-methylfuran from furfuryl alcohol. However, the reaction mixture immediately became tar-black and stuck at the bottom of the RBF.[77] This issue persisted even when the temperature of the solution was kept below 5 °C. Hence, to circumvent this issue, less reactive 2-chloromethyl furan was prepared using the method reported in the literature,[77,78] and the solvent was

evaporated below 10 °C. The isolated product was immediately reacted with 1,4-cyclohexanediol with one equivalent of sodium hydride to obtain mono-2-methylfuran-substituted-cyclohexanol. The obtained ether-alcohol substituted product was oxidized with pyridinium chlorochromate (PCC) to obtain the respective cyclohexanone derivative (**Figure S14**†). The Baeyer-Villiger oxidation of 2-methoxyfuran-cyclohexanone with *m*CPBA resulted in the desired FuCL monomer (^{1}H and ^{13}C NMR **Figures S15-S16**†).

Synthesis of homopolymer and block copolymer

To confirm the ability of the FuCL monomer to undergo ROP, homopolymerization was carried out using our previously reported method.[17,18] The benzyl alcohol and $Sn(Oct)_2$ were used as initiator and catalyst, respectively, and the reaction was carried out under a nitrogen atmosphere. A feed ratio 100:1:1 (monomer:catalyst:initiator) was used to obtain homopolymer (^{1}H and ^{13}C NMR **Figures S17-S18**†). The amphiphilic copolymers were synthesized similarly to homopolymer but using PEG_{2000} initiator (^{1}H, ^{13}C NMR, SEC **Figure S19-S21**†). The properties of homopolymer and block polymer are listed in **Table 2**.

Table 2. Properties of the obtained polyester using ^{1}H NMR and SEC.

Polymer	Monomer: Initiator	M_n[a] (g mol^{-1})	M_n[b] (g mol^{-1})	Dispersity (Đ)[b]
PFuCL	100:1	14200	8900	1.402
PEG-*b*-PFuCL	50:1	9800	6700	1.436

[a]Calculated from ^{1}H NMR analysis. [b]Calculated from SEC analysis.

Preparation and characterization of amphiphilic PEG-*b*-PFuCL micelles

Determination of Critical Micelle Concentration

The critical micelle concentration (CMC) is the minimum concentration of amphiphilic polymers required to undergo self-assembly in aqueous media. Micelles with lower CMC are considered thermodynamically stable and are desirable for drug delivery applications since they can withstand infinite dilution post injection *in vivo*.[79,80] Therefore, if the CMC of the amphiphilic polymer is high, the drug-loaded micelles, upon injection in the body, would fall apart and lead to premature release of the drug before reaching the target site. [79-81] The CMC of PEG-*b*-PFuCL was obtained by fluorescence spectroscopy using pyrene as a hydrophobic fluorescent probe.[17,69,70] As the concentration reaches CMC, the pyrene is encapsulated in the micelles, and the excitation peak of the pyrene shifts from 338 nm to 334 nm. The ratio of intensity at these wavelengths was plotted against the concentration of the polymer, and the intersection of the lines was taken as CMC (**Figure 8**). For the PEG-*b*-PFuCL, the CMC was found to be 1.78×10^{-3} mg mL^{-1} which is comparable to the micelles obtained from PEG-*b*-PBnCL.[16,18] This suggests that the PEG-*b*-PFuCL micelles are thermodynamically stable and capable of remaining intact upon dilution, preventing premature drug release due to dissociation.

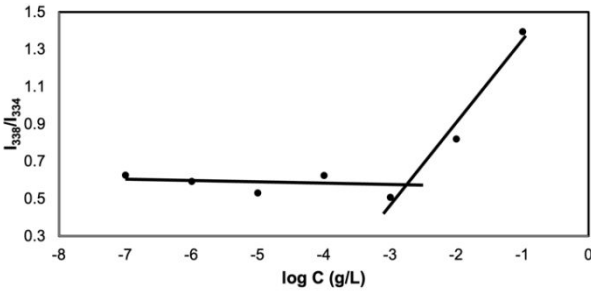

Figure 8. CMC of PEG-*b*-PFuCL using the fluorescent spectroscopy where the intensity ratio of pyrene is plotted against a log of polymer concentrations. The CMC of PEG-*b*-PFuCL was determined to be 1.78×10^{-3} mg mL^{-1}.

Size and Morphology of the Micelles

The prepared empty and DOX-loaded micelles were analyzed with dynamic light scattering (DLS) to evaluate hydrodynamic diameters. The size of the empty micelles was 54.28 nm, whereas the size of DOX-loaded micelles was 58.07 nm, respectively (**Figure 9A**). These sizes are in a similar range to micelle sizes obtained by other amphiphilic polymers reported by our group.[16,17,30,70] The aromatic groups present at the core of micelles promote the π–π interaction with aromatic DOX molecules, leading to the compact packing of encapsulated DOX molecules within the micelles.[16,51] This is consistent with R_g analysis of the simulated Fu-micelles where lower R_g values of micelles were observed for PEG-*b*-PFuCL micelles. Although an increase in micellar size was observed upon DOX encapsulation, the increase is negligible (~ 7%) compared to the reports where a larger increment upon drug encapsulation was observed.[16,30] As discussed in polymer-drug interaction analysis, MD

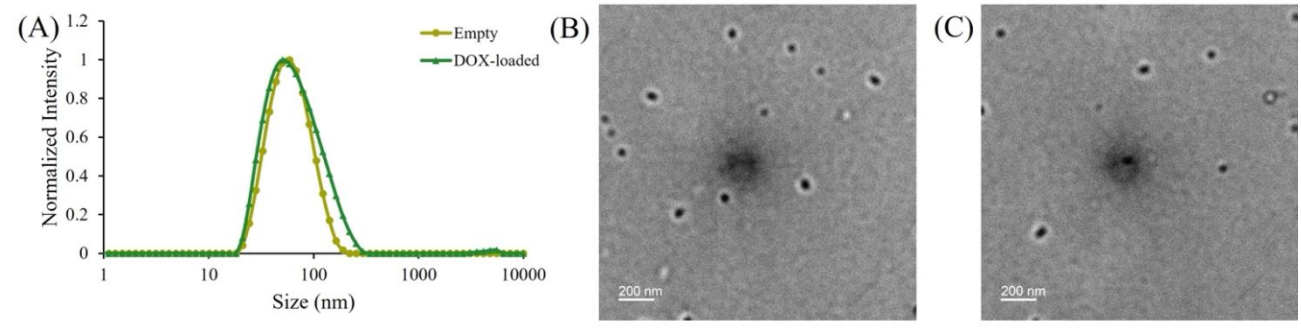

Figure 9. (A) DLS of empty and drug-loaded PEG-b-PFuCL micelles. TEM images of (B) empty and (C) drug-loaded PEG-b-PFuCL showed that the polymer formed spherical micelles.

simulation and related analyses showed that the Fu functional group is capable of interacting with DOX molecules via π–π interactions and hydrogen bonding, providing higher interaction with the incorporated DOX, with a tighter micellar packing, leading to an overall smaller micelle size. To determine the morphology of micelles, we carried out transmission electron microscopy (TEM) analysis **(Figures 9B-C**). The TEM images reveal that all the micelles have a spherical morphology, with sizes comparable to those obtained by DLS. Provided the size of DOX-loaded micelles is <100 nm, our micelles can passively accumulate in the tumor cells through the EPR effect.

Drug Loading Capacity and in vitro Drug Release

The capability of PEG-*b*-PFuCL micelles as a drug carrier was analyzed by encapsulating DOX as the hydrophobic anticancer drug. The encapsulation of the DOX in the hydrophobic core was achieved by a solvent exchange method, and micelles were dialyzed, as described in the experimental section. The drug loading capacity (DLC) of PEG-*b*-PFuCL micelles was 4.25% while the drug loading efficiency was 42.5%, respectively (**Table 3**). The DLC of PEG-*b*-PFuCL micelles is not only greater than pristine amphiphilic PCL micelles, but also better than PCL micelles containing aromatic and aliphatic functional groups reported recently.[16,18,33,82,83] The higher DLC of the PEG-*b*-PFuCL micelles can be attributed to π-electron and electrostatic interactions between DOX and functional Fu group. Our simulation studies also observed this interaction, where micelles containing the Fu functional group showed the highest interaction with DOX molecules.

Table 3. Size, DLC and DLE of the PEG-*b*-PFuCL micelles.

Micelles	Size (Đ) nm		Polymer:DOX	DLC (%)	DLE (%)
	Empty	Loaded			
PEG-*b*-PFuCL	54.28 (0.173)	58.07 (0.243)	10:1	4.25	42.5

After confirming the capability of our micelles to encapsulate drugs, we carried out the in vitro drug release studies. The release studies were conducted in PBS solution with physiological and endolysosomal pH (7.4 and 5.0, respectively) for 48 h (**Figure 10**). The acidic pH was chosen to simulate the overall acidic environment of the tumors, as reported in the literature.[5,19,84] The micelles released over 80% of the DOX within 24 h at acidic pH, while only 30% of the drug release was observed from the micelles kept at the physiological pH. Furthermore, the micelles at physiological pH released only ~40% of the encapsulated DOX at the end of the study. This discrepancy in the drug release could be due to the backbone of the PCL, which contains the hydrolysable ester bonds. The slower release from the micelles at physiological pH is also expected, given the stronger interactions between the hydrophobic core and drug molecules. The stronger interactions are suggested to diminish the release rate of the drug.[17,33,85] This slower drug release at the physiological pH suggests our micelles could circulate in the body with the minimum drug "leakage" in the bloodstream, reducing unwanted toxicity. This study confirms that the prepared micelles are stable and show a pH-dependent drug release behavior.

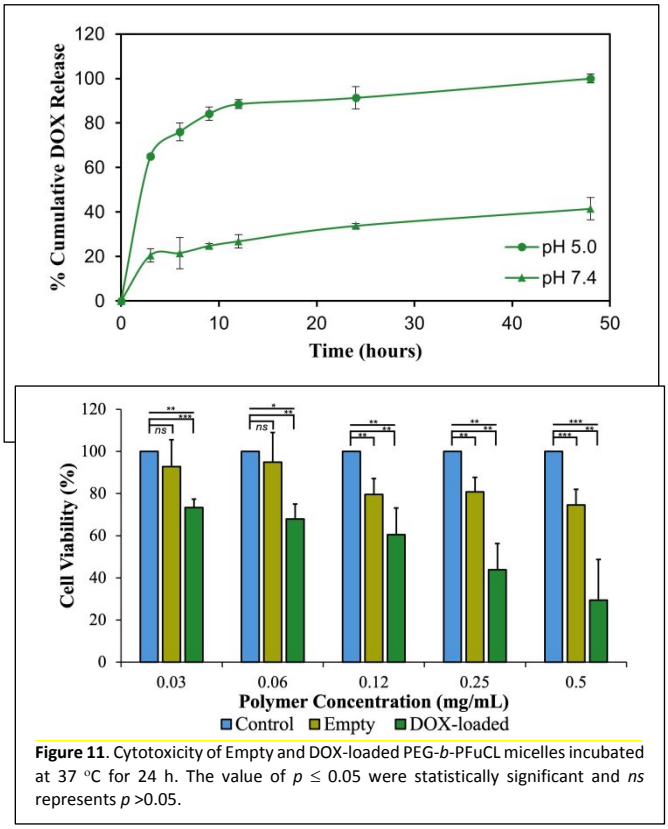

Figure 11. Cytotoxicity of Empty and DOX-loaded PEG-*b*-PFuCL micelles incubated at 37 °C for 24 h. The value of $p \leq 0.05$ were statistically significant and *ns* represents $p > 0.05$.

Biological Studies of the Micelles

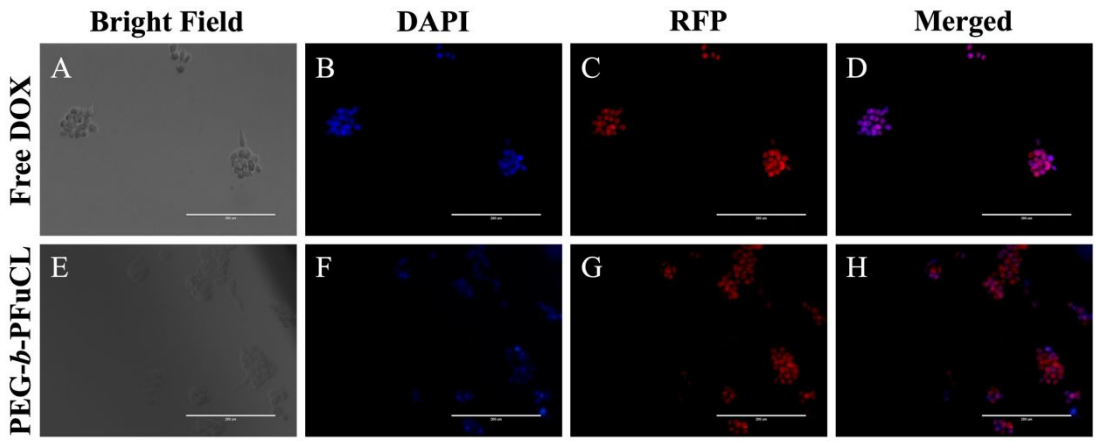

Figure 12. Cellular uptake of free DOX and PEG-*b*-PFuCL micelles into MDA-MB-231 cells at 37 °C after 4 h of incubation. Images of bright field, cells with nuclei staining using DAPI, DOX imaged with RFP filter, and merged image of DAPI and DOX (left to right). The scale bar is 200 μm.

Cytotoxicity of the micelles

The cytotoxicity of PEG-*b*-PFuCL micelles (empty and DOX-loaded) was assessed with MTT assay against the MDA-MB-231 breast cancer cells. The cells were exposed to various concentrations of micelles ranging from 0.03 to 0.5 mg mL^{-1}. The viability values demonstrated in **Figure 11** indicate that the empty micelles show a slight cytotoxicity to the cell, at the highest concentration, like the viability of empty PEG-*b*-PBnCL micelles reported by our group.[16] The highest cytotoxicity was observed from DOX-loaded micelles with a cell viability of 27% when treated with 0.5 mg mL^{-1} concentration. Interestingly, the cell viability at 0.25 mg mL^{-1} concentration is slightly higher than our previously reported DOX-loaded PEG-*b*-PBnCL micelles. This could be attributed to the fact that the drug release from the PEG-*b*-PFuCL micelles was much slower *in vitro* than that of the PEG-*b*-PBnCL micelles.[16,20]

Cellular uptake

Cellular uptake studies confirm that malignant cells passively uptake the drug-loaded micelles (**Figure 12**). To study this, MDA-MB-231 cells were plated in 24 well plate and dosed with DOX-loaded micelles for 4 h. After the incubation, the cells were fixed 4% paraformaldehyde and treated with DAPI to stain the nucleus. The cells were observed under EVOS FL digital inverted fluorescence microscope using DAPI (**Figure 12B-D**) and RFP (**Figure 12F-H**) filters, which shows the DOX-loaded micelles were primarily accumulated into the cells, and the DOX was internalized within the nuclei of the cells. The magenta color in merged image shows that the DOX-loaded micelles penetrate the cells presumably through endocytosis, with DOX primarily accumulating at the cell nuclei.

Conclusions

We performed all-atom MD simulations of four amphiphilic block copolymer micelles containing PEG as a hydrophilic block and poly(ε-caprolactone) functionalized at γ-position with cyclopentane, cyclopentadiene, furan, and thiophene functional groups as a hydrophobic block. The simulated polymers underwent aggregation to form a micelle and readily uptaken DOX. The SASA, watershell, and dehydration analysis shows the hydrophobic block of the micelles is tightly packed and prevents exposure to aqueous media. The SASA and watershell of the DOX molecules embedded in the micelles containing aromatic and diene groups are lesser than the cyclopentane group, suggesting these aromatic groups prevent encapsulated drug molecules from surrounding aqueous media. The interaction analysis shows the vdW forces are the major contributing interactions for drug encapsulation, with the furan group containing micelles showing the highest total interaction with DOX molecules due to its large electrostatic interactions. Further, NCI analysis shows that the micelles containing the Fu functional group formed more stable T-shaped and off-centered π–π stacking with furan groups within the polymeric chains and DOX molecules. Hence, from the MD trajectory analysis, furan functional group containing polymers performed the best, and we successfully synthesized γ-2-methoxyfuran-ε-caprolactone monomer. The synthesized amphiphilic block copolymer, PEG-*b*-PFuCL, readily undergoes self-assembly to form micelles with a DLC of 4.25 wt%. These nanoformulations are thermodynamically stable and show a triggered release at the acidic medium in vitro. The biological studies show that the micelles are biocompatible and readily uptaken by the breast cancer cells via EPR effect. In conclusion, we demonstrate the incorporation of MD simulations for the efficient design of micellar drug delivery carriers. These drug carriers have a straightforward synthesis, higher DLC and are capable of penetrating into cells *via* EPR effect. Future studies will be directed to utilize the furan functional group for post-polymerization modifications, such as the Diels-Alder reaction, to enhance the efficacy of the carrier.

Author contributions

T.S. carried out computational studies and synthesized monomers; H.P. synthesized polymers, prepared micelles, and conducted biological studies; G.B. optimized polymer:drug ratio, conducted drug release studies, and obtained TEM data; A.B. performed data analysis and reviewed manuscript, C.C.C.

performed UV-Vis and DLS experiments; G.G. assisted in monomer synthesis and purification; M.C.B. performed data analysis and reviewed manuscript; H.T. supervised computational section of the project; M.C.S supervised experimental section of the project; H.T. and M.C.S. designed the project; all the authors wrote manuscript together.

Conflicts of interest

The authors declare no conflict of interest.

Data availability

The supporting data for this article have been included in SI†. The input files, parameters, trajectories and other data will be provided upon request. Input files required for MD simulations are available at https://zenodo.org/records/14279583.

Acknowledgements

The authors acknowledge Shailendra Koirala for their assistance in cellular uptake images. T.S. and H.T. acknowledge Prof. Steven O. Nielsen for valuable suggestions on charge scaling. The authors acknowledge the Texas Advanced Computing Center (TACC) at the University of Texas at Austin, the Office of Information Technology, and Cyberinfrastructure Research Computing (CIRC) department at the University of Texas at Dallas for providing HPC resources that have contributed to the research results reported. H.T. acknowledges a startup grant from the University of Texas at Dallas. M.C.S. acknowledges financial support from the Welch Foundation (AT-1740) and the National Science Foundation (CHE-1609880). M. C. S. thanks the endowed chair support from the Eugene McDermott Foundation.

Notes and references

1 P. G. Fragouli, D. Stavroulaki, P. Christakopoulos, V. Athanasiou, M. Kasimati, K. Mathianaki and H. Iatrou, in *Stimuli Responsive Polymeric Nanocarriers for Drug Delivery Applications*, Elsevier, 2019, pp. 439-460.
2 Y. Zhong, F. Meng, C. Deng and Z. Zhong, *Biomacromolecules*, 2014, **15**, 1955-1969.
3 Q. Zhou, L. Zhang, T. Yang and H. Wu, *Int. J. Nanomedicine*, 2018, **13**, 2921-2942.
4 J. Hao, J. Servello, P. Sista, M. C. Biewer and M. C. Stefan, *J. Mater. Chem.*, 2011, **21**, 10623-10628.
5 A. Bhadran, T. Shah, G. K. Babanyinah, H. Polara, S. Taslimy, M. C. Biewer and M. C. Stefan, *Pharmaceutics*, 2023, **15**, 1977.
6 T. V. Shah and D. V. Vasava, *e-Polymers*, 2019, **19**, 385-410.
7 Z. Shariatinia and A. Mazloom-Jalali, *J. Mol. Liq.*, 2019, **273**, 346-367.
8 M. A. Woodruff and D. W. Hutmacher, *Prog. Polym. Sci.*, 2010, **35**, 1217-1256.
9 L. S. Nair and C. T. Laurencin, *Prog. Polym. Sci.*, 2007, **32**, 762-798.
10 E. A. Rainbolt, K. E. Washington, M. C. Biewer and M. C. Stefan, *Polym. Chem.*, 2015, **6**, 2369-2381.
11 A. M. Jhaveri and V. P. Torchilin, *Front. Pharmacol.*, 2014, **5**, 77.
12 C. Deng, Y. J. Jiang, R. Cheng, F. H. Meng and Z. Y. Zhong, *Nano Today*, 2012, **7**, 467-480.
13 Z. Ahmad, A. Shah, M. Siddiq and H. B. Kraatz, *RSC Adv.*, 2014, **4**, 17028-17038.
14 T. T. Chen, T. J. Cai, Q. Jin and J. Ji, e-*Polymers*, 2015, **15**, 3-13.
15 S. Gautier, V. D'Aloia, O. Halleux, M. Mazza, P. Lecomte and R. Jerome, *J. Biomater. Sci. Polym. Ed.*, 2003, **14**, 63-85.
16 K. E. Washington, R. N. Kularatne, M. C. Biewer and M. C. Stefan, *ACS Biomater. Sci. Eng.*, 2018, **4**, 997-1004.
17 A. Bhadran, H. Polara, E. L. Calubaquib, H. Wang, G. K. Babanyinah, T. Shah, P. A. Anderson, M. Saleh, M. C. Biewer and M. C. Stefan, *Biomacromolecules*, 2023, **24**, 5823-5835.
18 G. K. Babanyinah, A. Bhadran, H. Polara, H. Wang, T. Shah, M. C. Biewer and M. C. Stefan, *Chem. Sci.*, 2024, **15**, 9987-10001.
19 19. S. A. Senevirathne, K. E. Washington, J. B. Miller, M. C. Biewer, D. Oupicky, D. J. Siegwart and M. C. Stefan, *J. Mater. Chem. B*, 2017, **5**, 2106-2114.
20 P. Soltantabar, E. L. Calubaquib, E. Mostafavi, M. C. Biewer and M. C. Stefan, *Biomacromolecules*, 2020, **21**, 1427-1436.
21 R. N. Kularatne, K. E. Washington, C. Bulumulla, E. L. Calubaquib, M. C. Biewer, D. Oupicky and M. C. Stefan, *Biomacromolecules*, 2018, **19**, 1082-1089.
22 J. Hao, P. C. Granowski and M. C. Stefan, *Macromol. Rapid Commun.*, 2012, **33**, 1294-1299.
23 A. Sosnik and M. Menaker Raskin, *Biotechnol. Adv.*, 2015, **33**, 1380-1392.
24 I. Negut and B. Bita, *Pharmaceutics*, 2023, **15**, 976.
25 S. H. Wang, K. M. Cheng, K. Chen, C. Xu, P. W. Ma, G. H. Dang, Y. Q. Yang, Q. Lei, H. Y. Huang, Y. Yu, Y. Fang, Q. Y. Tang, N. Jiang, H. L. Miao, F. A. Liu, X. Zhao and N. Li, *Nano Today*, 2022, **45**, 101512.
26 M. Cagel, F. C. Tesan, E. Bernabeu, M. J. Salgueiro, M. B. Zubillaga, M. A. Moretton and D. A. Chiappetta, *Eur. J. Pharm. Biopharm.*, 2017, **113**, 211-228.
27 C. Yang, A. B. Attia, J. P. Tan, X. Ke, S. Gao, J. L. Hedrick and Y. Y. Yang, *Biomaterials*, 2012, **33**, 2971-2979.
28 C. K. McLaughlin, J. Logie and M. S. Shoichet, *Isr. J. Chem.*, 2013, **53**, 670-679.
29 W. R. Zhuang, Y. Wang, P. F. Cui, L. Xing, J. Lee, D. Kim, H. L. Jiang and Y. K. Oh, *J. Control. Release.*, 2019, **294**, 311-326.
30 H. Wang, H. Polara, A. Bhadran, T. Shah, G. K. Babanyinah, Z. Ma, E. L. Calubaquib, J. T. Miller, M. C. Biewer and M. C. Stefan, *Front. Pharmacol.*, 2024, **15**, 1356639.
31 Y. Shi, M. J. van Steenbergen, E. A. Teunissen, L. Novo, S. Gradmann, M. Baldus, C. F. van Nostrum and W. E. Hennink, *Biomacromolecules*, 2013, **14**, 1826-1837.
32 V. Karmegam, S. S. Kuruppu, C. M. Udamulle Gedara, M. C. Biewer and M. C. Stefan, *J. Polym. Sci.*, 2021, **59**, 3040-3052.
33 S. Buwalda, A. Al Samad, A. El Jundi, A. Bethry, Y. Bakkour, J. Coudane and B. Nottelet, *J. Colloid Interface Sci.*, 2018, **514**, 468-478.
34 Z. Wu, M. Duan, D. Xiong and C. Y. Zhang, *Pharmaceutics*, 2019, **11**, 620.
35 J. Kehrein, A. Bunker and R. Luxenhofer, *Mol. Pharm.*, 2024, **21**, 3356-3374.
36 36. S. Kotta, H. M. Aldawsari, S. M. Badr-Eldin, A. B. Nair and K. YT, *Pharmaceutics,* 2022, **14**, 1636.
37 T. Duran, A. Costa, A. Gupta, X. Xu, H. Zhang, D. Burgess and B. Chaudhuri, *Mol. Pharm.*, 2022, **19**, 1117-1134.
38 M. Bhendale and J. K. Singh, *Langmuir*, 2023, **39**, 5031-5040.
39 W. Wu, Z. Zou, S. Yang, Q. Wu, W. Li, Q. Ding, Z. Guan and W. Zhu, *Langmuir*, 2020, **36**, 2082-2092.
40 L. S. Zheng, Y. Q. Yang, X. D. Guo, Y. Sun, Y. Qian and L. J. Zhang, *J. Colloid Interface Sci.*, 2011, **363**, 114-121.
41 N. Razavilar and G. Hanna, *Macromol. Theory Simul.*, 2022, **31**, 2100060.
42 H. Kuramochi, Y. Andoh, N. Yoshii and S. Okazaki, *J. Phys. Chem. B*, 2009, **113**, 15181-15188.

43 M. Rezaeisadat, A. K. Bordbar and R. Omidyan, *J. Mol. Liq.*, 2021, **332**, 115862.
44 T. Shah, M. C. Stefan and H. Torabifard, *J. Phys. Chem. B*, 2024, **128**, 11981-11991.
45 E. Kabir and M. Uzzaman, *Results Chem.*, 2022, **4**, 100606.
46 J. Alvarez-Builla, J. J. Vaquero and J. Barluenga, *Modern heterocyclic chemistry*, Wiley Online Library, 2011.
47 R. Dua, S. Shrivastava, S. K. Sonwane and S. K. Srivastava, *Advances in Biological Research*, 2011, **5**, 120-144.
48 A. Gomtsyan, *Chemistry of Heterocyclic Compounds*, 2012, **48**, 7-10.
49 P. Martins, J. Jesus, S. Santos, L. R. Raposo, C. Roma-Rodrigues, P. V. Baptista and A. R. Fernandes, *Molecules*, 2015, **20**, 16852-16891.
50 E. A. Rainbolt, J. B. Miller, K. E. Washington, S. A. Senevirathne, M. C. Biewer, D. J. Siegwart and M. C. Stefan, *J. Mater. Chem. B*, 2015, **3**, 1779-1787.
51 J. Hao, Y. X. Cheng, R. J. K. U. Ranatunga, S. Senevirathne, M. C. Biewer, S. O. Nielsen, Q. Wang and M. C. Stefan, *Macromolecules*, 2013, **46**, 4829-4838.
52 R. Dennington, T. A. Keith and J. M. Millam, *GaussView, Version 6. Semichem Inc.*, Shawnee Mission, 2019.
53 M. J. Frisch, G. W. Trucks, H. B. Schlegel, G. E. Scuseria, M. A. Robb, J. R. Cheeseman, G. Scalmani, V. Barone, G. A. Petersson, H. Nakatsuji, X. Li, M. Caricato, A. V. Marenich, J. Bloino, B. G. Janesko, R. Gomperts, B. Mennucci, H. P. Hratchian, J. V. Ortiz, A. F. Izmaylov, J. L. Sonnenberg, D. Williams-Young, F. Ding, F. Lipparini, F. Egidi, J. Goings, B. Peng, A. Petrone, T. Henderson, D. Ranasinghe, V. G. Zakrzewski, J. Gao, N. Rega, G. Zheng, W. Liang, M. Hada, M. Ehara, K. Toyota, R. Fukuda, J. Hasegawa, M. Ishida, T. Nakajima, Y. Honda, O. Kitao, H. Nakai, T. Vreven, K. Throssell, J. A. Montgomery, Jr., J. E. Peralta, F. Ogliaro, M. J. Bearpark, J. J. Heyd, E. N. Brothers, K. N. Kudin, V. N. Staroverov, T. A. Keith, R. Kobayashi, J. Normand, K. Raghavachari, A. P. Rendell, J. C. Burant, S. S. Iyengar, J. Tomasi, M. Cossi, J. M. Millam, M. Klene, C. Adamo, R. Cammi, J. W. Ochterski, R. L. Martin, K. Morokuma, O. Farkas, J. B. Foresman and D. J. Fox, *Gaussian~16 Revision C.01*, 2016, Gaussian Inc. Wallingford CT.
54 J. Wang, R. M. Wolf, J. W. Caldwell, P. A. Kollman and D. A. Case, *J. Comput. Chem.*, 2004, **25**, 1157-1174.
55 J. Wang, W. Wang, P. A. Kollman and D. A. Case, *J. Am. Chem. Soc.*, 2001, **222**, 2001.
56 A. Jakalian, B. L. Bush, D. B. Jack and C. I. Bayly, *J. Comput. Chem.*, 2000, **21**, 132-146.
57 A. Jakalian, D. B. Jack and C. I. Bayly, *J. Comput. Chem.*, 2002, **23**, 1623-1641.
58 L. Martinez, R. Andrade, E. G. Birgin and J. M. Martinez, *J. Comput. Chem.*, 2009, **30**, 2157-2164.
59 W. L. Jorgensen, J. Chandrasekhar, J. D. Madura, R. W. Impey and M. L. Klein, *J. Chem. Phys.*, 1983, **79**, 926-935.
60 D. A. Case, K. Belfon, I. Y. Ben-Shalom, S. R. Brozell, D. S. Cerutti, T. E. Cheatham III, V. W. D. Cruzeiro, T. A. Darden, R. E. Duke, G. Giambasu, M. K. Gilson and Other, *Amber 2020*, University of California, San Francisco, 2020.
61 R. J. Loncharich, B. R. Brooks and R. W. Pastor, *Biopolymers*, 1992, **32**, 523-535.
62 H. J. C. Berendsen, J. P. M. Postma, W. F. Vangunsteren, A. Dinola and J. R. Haak, *J. Chem. Phys.*, 1984, **81**, 3684-3690.
63 J.-P. Ryckaert, G. Ciccotti and H. J. C. Berendsen, *J. Comput. Phys.*, 1977, **23**, 327-341.
64 U. Essmann, L. Perera, M. L. Berkowitz, T. Darden, H. Lee and L. G. Pedersen, *J. Chem. Phys.*, 1995, **103**, 8577-8593.
65 W. Humphrey, A. Dalke and K. Schulten, *J. Mol. Graph.*, 1996, **14**, 33-38, 27-38.
66 D. R. Roe and T. E. Cheatham, 3rd, *J. Chem. Theory Comput.*, 2013, **9**, 3084-3095.
67 N. K. Li, Y. Xie and Y. G. Yingling, *J. Phys. Chem. B*, 2021, **125**, 8627-8635.
68 T. Lu and F. Chen, *J. Comput. Chem.*, 2012, **33**, 580-592.
69 J. Aguiar, P. Carpena, J. A. Molina-Bolívar and C. C. Ruiz, *J. Colloid Interface Sci.*, 2003, **258**, 116-122.
70 H. Wang, E. L. Calubaquib, A. Bhadran, Z. Ma, J. T. Miller, A. Zhang, M. C. Biewer and M. C. Stefan, *Polym. Chem.*, 2023, **14**, 514-522.
71 L. Razavi, H. Raissi and F. Farzad, *Sci. Rep.*, 2023, **13**, 2665.
72 L. Huynh, C. Neale, R. Pomès and C. Allen, *Soft Matter*, 2010, **6**, 5491-5501.
73 A. O. Kasimova, G. M. Pavan, A. Danani, K. Mondon, A. Cristiani, L. Scapozza, R. Gurny and M. Moller, *J. Phys. Chem. B*, 2012, **116**, 4338-4345.
74 R. G. Huber, M. A. Margreiter, J. E. Fuchs, S. von Grafenstein, C. S. Tautermann, K. R. Liedl and T. Fox, *J. Chem. Inf. Model*, 2014, **54**, 1371-1379.
75 E. R. Johnson, S. Keinan, P. Mori-Sanchez, J. Contreras-Garcia, A. J. Cohen and W. Yang, *J. Am. Chem. Soc.*, 2010, **132**, 6498-6506.
76 C. R. Martinez and B. L. Iverson, *Chem. Sci.*, 2012, **3**, 2191-2201.
77 W. R. Kirner, *J. Am. Chem. Soc.*, 2002, **50**, 1955-1961.
78 S. Senaweera and J. D. Weaver, *Chem. Commun.*, 2017, **53**, 7545-7548.
79 L. I. Atanase, *Polymers*, 2021, **13**, 477.
80 M. Ghezzi, S. Pescina, C. Padula, P. Santi, E. Del Favero, L. Cantu and S. Nicoli, *J. Control. Release*, 2021, **332**, 312-336.
81 A. Rahmani, F. Rahimi, M. Iranshahi, H. Kahroba, A. Zarebkohan, M. Talebi, R. Salehi and H. Z. Mousavi, *Sci. Rep.*, 2021, **11**, 21425.
82 A. El Jundi, S. Buwalda, A. Bethry, S. Hunger, J. Coudane, Y. Bakkour and B. Nottelet, *Biomacromolecules*, 2020, **21**, 397-407.
83 M. Malhotra, B. Surnar and M. Jayakannan, *Macromolecules*, 2016, **49**, 8098-8112.
84 S. A. Senevirathne, S. Boonsith, D. Oupicky, M. C. Biewera and M. C. Stefan, *Polym. Chem.*, 2015, **6**, 2386-2389.
85 G. Kang, L. Sun, Y. Liu, C. Meng, W. Ma, B. Wang, L. Ma, C. Yu and H. Wei, *Langmuir*, 2019, **35**, 12509-12517.

Data availability

The supporting data for this article have been included in SI†. The input files, parameters, trajectories and other data will be provided upon request. Input files required for MD simulations are available at https://zenodo.org/records/14279583.